Tailoring the properties of BaTi$_{0.8}$Cu$_{0.2}$O$_3$ catalyst selecting the synthesis method.

Vicente Albaladejo-Fuentes[a], Franz Edwin López-Suárez[b], María Salvadora Sánchez-Adsuar[a], María José Illán-Gómez[a,*]

[a]*Carbon Materials and Environment Research Group, Department of Inorganic Chemistry, Faculty of Science, Universidad de Alicante, Alicante, Spain*

[b]*Instituto Colombiano del Petróleo - ICP, Ecopetrol S.A., Km 7 vía a Piedecuesta, Piedecuesta, Colombia.*

corresponding author: illan@ua.es. Phone: +34965903975.
Department of Inorganic Chemistry, Faculty of Science, Universidad de Alicante, Av. Alicante s/n, 03690, San Vicente del Raspeig, Alicante, Spain

Highlights

- BaTiO$_3$ and BaTi$_{0.8}$Cu$_{0.2}$O$_3$ perovskites were synthesized using sol-gel and hydrothermal methods.

- The location of copper in the catalyst depends on the synthesis method.

- Cu-BTOsg, with Cu incorporated into the structure, presents a high NOx storage capacity.

- Cu-BBOH, with CuO highly dispersed on the surface, shows a high activity for NO to NO$_2$ oxidation.

Abstract

The effect of the synthesis method (hydrothermal and sol-gel) on the properties of $BaTi_{0.8}Cu_{0.2}O_3$ perovskites as catalysts for NOx and soot removal has been analyzed. X-ray powder diffraction (XRD), X-ray Photoelectron Spectroscopy (XPS), ICP-AES, N_2 adsorption at -196ºC, Raman spectroscopy, Field Emission Scanning Electron Microscopy (FESEM) and temperature programmed reduction with hydrogen (H_2-TPR) have been used for catalysts characterization. To test their catalytic activity, NOx storage and soot combustion temperature programmed reaction tests have been carried out.

The results allow to conclude that the synthesis method determines the position of copper on the perovskite structure and, therefore, the catalytic applications. When the hydrothermal method is used the copper is highly dispersed on the perovskite surface, obtaining a catalyst with a high activity for the NO to NO_2 oxidation reaction, which can be used as oxidation catalyst for soot removal. Nevertheless, using the sol-gel method, copper is incorporated into the perovskite structure and, consequently, the catalyst presents a high NOx storage capacity

I. Introduction

Barium titanate ($BaTiO_3$) is one of the best known and currently used materials in ceramic and electronic industries due to its excellent dielectric, ferroelectric, and piezoelectric properties, which come from its unique perovskite structure (ABO_3) [1–3]. $BaTiO_3$ has also been used as catalyst for oxidation and dry reforming of methane [4–6], for NOx reduction [7], as photocatalyst for hydrogen production [8] and for toluene degradation [9] and, finally, its properties have been checked for biomedical applications [10,11]. The extensive use of perovskite-type mixed-metal oxides as catalysts and/or as catalyst supports is due to their ability to provide high (lattice) oxygen mobility and also high structural stability [12]. The performance of $BaTiO_3$ depends mainly on the crystal structure, shape, size, stoichiometry, homogeneity and surface properties, which are determined by the synthesis method [7,13].

To prepare $BaTiO_3$, a wide variety of synthetic methods have been proposed, including conventional solid-state synthesis [14], co-precipitation [15], micro-emulsion method [16–18], spray pyrolysis [19], oxalate route [20], hydrothermal method [21–26], microwave-hydrothermal method [27,28], and sol‑gel method [1,29,30] among others. The conventional solid-state synthesis typically involves high-temperature calcinations (1200°C) of a $BaCO_3$ and TiO_2 powder mixture, which often results in low purity and polydispersity of the final structure due to the high reaction temperature and heterogeneous solid-phase reactions [14]. Therefore, the most popular methods for preparing $BaTiO_3$ perovskites are low temperature wet-chemistry methods, such as hydrothermal and sol‑gel.

The sol–gel method includes a first step where elemental mixing is achieved, followed by a firing step to burn off the complexing ligands and to induce crystallinity, therefore, the catalyst

preparation using a sol‑gel method is a complex process. However, it presents the following advantages: i) avoids the materials contamination, ii) allows a better shape control, iii) requires low capital investment and iv) can be compatible with continuous manufacturing techniques for the production of powders [29,31,32].

The hydrothermal crystallization of barium titanate is performed from aqueous mixtures of barium and titanium precursor salts. This process is carried out at pH values higher than 7 and temperatures above 80ºC for periods of time ranging from hours to a few days. Compared to conventional methods, the hydrothermal method is a low-temperature, low-cost and scalable technology, which can yield homogeneous particles of various shapes in the nano-scale size [33,34].

The substitution of cations in perovskites lattice allows improving the properties of these mixed-metal oxides for catalyst applications [12,35,36]. In a previous preliminary study [37], titanium was partially substituted by copper [38,39] in the $BaTiO_3$ perovskite structure, showing the resulting $BaTi_{1-x}Cu_xO_3$ perovskites a high activity for NOx storage, which was attributed to the presence of oxygen vacancies created on the catalyst surface as a consequence of the copper incorporation into the structure. It was also concluded that for $BaTi_{0.8}Cu_{0.2}O_3$ catalyst the NOx storage capacity increases with the copper content until a certain limit is reached. Moreover, this catalyst presents a NOx storage capacity (300 µmol/g at 420ºC) in the range of levels reported for noble metal-based catalysts [26]. Thus, the $BaTi_{0.8}Cu_{0.2}O_3$ catalyst has been selected to analyze the effect of synthesis method.

Nowadays, NOx and soot removal from lean-burn engines is a highly challenging issue. On the one hand, regarding NOx abatement, several technologies, as selective catalytic reduction (ammonia/urea-SCR and hydrocarbon-SCR) and NOx storage-reduction (NSR) have been

developed during the last decades [40]. Despite some drawbacks (such as a fuel penalty for rich events, sensitivity to fuel sulphur levels, thermal stability and control under transient engine operation [41]), NSR is still considered the most promising technology as it provides high de-NO_x performance and it does not require new infrastructure [42]. On another hand, the Diesel Particulate Filters (DPF) technology is employed for soot removal from the exhaust [40] and different materials (including simple and mixed transition metals oxides) [43,44] can be used as catalytic coating to decrease the temperature required to regenerate the filter.

In this paper, the effect of the $BaTi_{0.8}Cu_{0.2}O_3$ perovskites synthesis method on their properties as catalysts for NOx and soot removal has been analysed. Both a hydrothermal and a sol-gel method have been used to prepare $BaTiO_3$ and $BaTi_{0.8}Cu_{0.2}O_3$ perovskites. For the hydrothermal method, the effect of barium precursor- which can play a key role in the growth mechanism of $BaTiO_3$ during synthesis- has been considered.

II. Experimental

II.1 Catalysts synthesis method

Sol-gel method

$BaTiO_3$ and $BaTi_{0.8}Cu_{0.2}O_3$ were prepared using a sol-gel method based on the Pechini-type reaction route modified to be used in an aqueous media [37]. In brief, the titanium isopropoxide (Ti) was hydrolysed and the resulting specie was solved in an aqueous solution of citric acid (CA) (Ti:CA = 1:2) and hydrogen peroxide (Ti:H_2O_2 = 2:1), forming the citrate-peroxo-titanate (IV) complex. Afterwards, the pH was adjusted to 8.5 with NH_3, and the barium (Ba:Ti = 1:1) and copper precursor were added, using the amount corresponding to the stoichiometry ($BaTi_{0.8}Cu_{0.2}O_3$). The solution was kept at 65ºC for 5h, until a gel was obtained. Then, the

sample was dried at 90ºC for 24h and, finally, calcined at 850ºC for 6h. The $BaTiO_3$ and $BaTi_{0.8}Cu_{0.2}O_3$ materials prepared by sol-gel method are called BTOsg and Cu-BTOsg, respectively (Table 1).

Hydrothermal method

$BaTiO_3$ and $BaTi_{0.8}Cu_{0.2}O_3$ were also synthesized by a hydrothermal method [26]. First of all, the barium precursor (barium acetate, nitrate or hydroxide) was dissolved in the appropriate volume of water and placed in a 50 mL Teflon vessel for 1 hour at 90ºC. The titanium and/or copper reactants were added to the barium solution as well as the adequate amount of the precipitant agent (mineralizer). The resulting mixture was placed again in a furnace at 90ºC. After reacting for 72 h, the vessel was taken out and cooled down to room temperature. The resultant products were filtered, washed with deionized water, dried in air at 90ºC and then calcined at 500ºC for 3h. Two mineralizers (sodium or potassium hydroxide) were tested to prepare $BaTiO_3$ and $BaTi_{0.8}Cu_{0.2}O_3$ materials when barium acetate or nitrate were the barium precursor. However, when barium hydroxide was used as barium precursor, not additional mineralizer was added. In Table 1, the precursor used for the synthesis and the nomenclature of the catalysts are shown.

II.2 Catalysts characterization

The copper content of the catalysts was measured by ICP-AES, using a Perkin–Elmer device, model Optimal 4300 DV. The metal was extracted from the catalysts by refluxing them in 8M HCl solution for 2h.

The BET surface areas were determined by physical adsorption of N_2 at -196ºC in an automatic volumetric system (Autosorb-6B from Quantachrome) after degassing the samples at 250ºC for 4h.

For the identification of phases and crystalline structures, X-ray diffraction (XRD) and Raman spectroscopy were used. XRD experiments were carried out on a Rigaku Miniflex II powder diffractometer, using Cu Kα (0,15418 nm) radiation with the 2θ angle in the range 20 to 80º, with a step of 0.025º and a time per step of 2 seconds. Raman scattering spectra were obtained on a Jobin-Ivon dispersive Raman spectrometer (model LabRam) with a variable power He:Ne laser source (633 nm) in the range of 100–1000 nm.

For XPS spectra, a K-Alpha Photoelectron Spectrometer (from Thermo-Scientific with a AlKα (1486.7 eV) radiation source) was used. For the analysis, the pressure of the analysis chamber was maintained at $5 \cdot 10^{-10}$ mbar. The binding energy (BE) and kinetic energy (KE) scales were adjusted by setting the C 1s transition at 284.6 eV, and the BE and KE values were then determined with the peak-fit software of the spectrometer.

The morphology of samples was observed with a ZEISS Merlin VP Compact Field Emission Scanning Electron Microscopy (FESEM) equipment.

Temperature programmed reduction experiments with H_2 (H_2-TPR) were carried out in a Micromeritics device (model Pulse ChemiSorb 2705). For the experiments, 20 mg of the sample were heated at 10ºC/min from 25 to 900ºC under a 5% H_2/Ar flow (40 ml/min, Ptotal = 1 atm).

II.3 Catalytic activity tests: NOx storage and soot combustion

Soot combustion and NOx storage tests were carried out under temperature programmed reaction (TPR) conditions from 25 to 800 °C, at 10 °C/min. Soot oxidation experiments were performed in a fixed-bed reactor at atmospheric pressure under a gas flow (500 ml/min,) containing 500 ppm NO_x, 5 % O_2 and balance N_2. The catalytic bed was composed by a soot-catalyst mixture (80 mg of catalyst + 20 mg of soot in loose contact + 300 mg SiC). The model soot used is a carbon black from Cabot (Printex U). NOx adsorption/desorption experiments were also performed under similar conditions but without soot. The gas composition as a function of temperature was monitored by specific NDIR-UV gas analysers for NO, NO_2, CO, CO_2 and O_2 (Rosemount Analytical Model BINOS 1001, 1004 and 100)

III. Results and discussion

III.1 Structural characterization by XRD and Raman spectroscopy.

Fig.1a and b show the XRD patterns of $BaTiO_3$ and $BaTi_{0.8}Cu_{0.2}O_3$ obtained by using the two synthesis methods. As it was expected, the perovskite structure [33] is the main phase for all $BaTiO_3$ mixed oxides (with or without copper) since the diffraction peaks observed (at 2Ɵ: 22,3º; 31,4º; 38,8º; 45,2º; 51,0º; 56,1º; 65,8º; 74,9º; for (100), (110), (111), (200), (210), (211), (220) and (310) lattice planes, respectively) correspond to the standard JCPDS: 5-626 [45].

In the XRD patterns of the BTOsg catalyst (Fig.1a), a weak peak at 23.7º is identified indicating the presence of $BaCO_3$ as segregated phase formed by carbonation of the excess of barium oxide during samples atmospheric exposure [39,46]. For the BAKOH, BNKOH and BBON catalysts, the presence of segregated phases is not identified. However, for BASOH and BNSOH (obtained

8

using NaOH as mineralizer) the presence of barium silicon titanium oxide ($Ba_2SiTi_2O_8$) -coming from the reaction between the barium and titanium precursors and the porcelain crucible used for the synthesis- is detected.

When a copper precursor is used in the sol-gel method to prepare the Cu-BTOsg catalyst, the presence of additional minority phases - such as Ba_2TiO_4 (28.7º, 28.8º, 29.3º, 30.1º), CuO (35.6º) and TiO_2 (as rutile phase at ca. 27.5º and 36.1º)- is observed in the XRD patterns (Fig.1b). However, the perovskite structure is still the main phase. As it was previously reported, the high fraction of segregated phases formed during the sol-gel synthesis of the copper catalysts [37] proves that copper was incorporated into the perovskite structure. For Cu-BAKOH, Cu-BASOH, Cu-BNKOH, Cu-BNSOH, and Cu-BBOH catalysts, only the diffraction peaks corresponding to CuO are observed. These peaks show a higher intensity than for Cu-BTOsg catalyst because a higher fraction of CuO seems to be present on the solid surface [36].

From the XRD results it can be concluded that the synthesis method determines the phases formed and the location of copper in the perovskite structure. When a sol-gel method is used more phases are detected due to the incomplete reaction among precursors and to the partial incorporation of copper into the perovskite structure. When the catalysts are obtained using the hydrothermal method, the reaction between titanium and barium precursors to form $BaTiO_3$ perovskite is almost completed, therefore, the unique additional diffraction peak identified corresponds to CuO, which seems to be highly dispersed on the surface of the $BaTiO_3$ perovskite. Additionally, it can be concluded that barium hydroxide is the most convenient barium precursor for the hydrothermal method, since it keeps the high pH required for the synthesis of high purity $BaTiO_3$ crystals [15] without using an additional alkaline mineralizer. Therefore, the $BaTiO_3$ and $BaTi_{0.8}Cu_{0.2}O_3$ perovskite prepared by sol-gel (BTOsg, Cu-BTOsg)

and by hydrothermal method using $Ba(OH)_2$ (BBOH, Cu-BBOH) have been selected to carry out a deep study of the effect of the synthesis method on the physico-chemical properties of the catalysts.

The Scherrer equation [47] was used to calculate the average crystal size for the BTOsg, BBOH, Cu-BTOsg and Cu-BBOH catalysts, which is shown in Table 2. A higher average crystal size is observed for the BBOH than for the BTOsg catalysts suggesting that, using the hydrothermal method, a mixed oxide with higher crystallinity is obtained. For copper catalysts, the average crystal size depends on the synthesis method. Using the sol-gel method (Cu-BTOsg), an increase of the crystal size is observed due to the incorporation of copper into the perovskite structure, whilst when the hydrothermal route is employed (Cu-BBOH), the crystal size decreases suggesting a lower crystallinity. As it was previously reported [37], by comparing the FWHM of the (2 0 0) and (1 1 1) XRD peaks, it is possible to determine if a perovskite presents a cubic or a tetragonal structure based on the (2 0 0)/(1 1 1) FWHM ratio. (This value is higher than 1 for a tetragonal perovskite structure due to the (0 0 2) peak of the tetragonal structure can appear overlapped with the (2 0 0) peak [48,49].) In Table 2 it is observed that the FWHM (2 0 0)/(1 1 1) ratio is higher than 1 for all selected catalysts, so, it could be concluded that tetragonal perovskite structure is adopted using the two synthesis methods. The lattice parameters a and c, corresponding to the tetragonal structure, were calculated using Difracc plus software® (by Bruker), and the data are also included in Table 2. For the Cu-BTOsg catalyst, the parameter a increases and the paramater c decreases with respect to the BTOsg catalyst, suggesting a distortion of the tetragonal structure due to copper incorporation into the perovskite structure. For the Cu-BBOH catalyst, both lattice parameters decrease respect to the BBOH probably due

to the understoichiometric amount of titanium used during the synthesis in order to promote the introduction of copper into the structure.

According to literature [49,50], only the tetragonal structure of $BaTiO_3$ perovskite, which belongs to space group *P4mm*, presents first-order Raman-active modes with bands at, approximately, 180 cm^{-1}, 265 cm^{-1},305 cm^{-1}, 520 $cm^{-1}$and 720 cm^{-1}, corresponding to irreducible representations (A1(LO)), (A1(TO)), (B1), (A1, E(TO)) and (A1, E(LO), respectively. The Raman spectra shown in Fig.2, confirm that the two bare perovskites (BTOsg, BBOH) present tetragonal perovskite structure since bands at 305 cm^{-1}, 520 cm^{-1} and 720 cm^{-1} are clearly observed. The addition of copper during the sol-gel synthesis (Cu-BTOsg) leads to a distortion of the tetragonal structure as the main peaks in the Raman spectrum (305 cm^{-1}, 520 $cm^{-1}$and 720 cm^{-1}) almost disappear and, in addition, a new band at ca. 750 cm^{-1}, corresponding to a Ba_2TiO_4 phase, is detected [51]. These results support the conclusion obtained from the XRD data (Fig.1b), and confirm that copper is introduced into the perovskite structure of the sol-gel catalyst. For the Cu-BBOH catalyst, a dramatic broadening of the tetragonal perovskite peaks is observed (Fig.2), indicating that the tetragonal structure is also modified. However, according with the XRD results (Fig.1a), the distorsion of the perovskite structure for Cu-BBOH catalyst seems to be related with the understoichiometric amount of titanium used during the synthesis.

III.2. Copper content, surface area and morphology.

The BET surface area (obtained from N_2 adsorption isotherm) and the copper content (measured by ICP-AES) of the catalysts are includedin Table 2. All catalysts show a low BET surface area, as it was expected for mixed oxides with perovskite structure [12,52]. The ICP-AES results reveal that all copper added for both synthesis methods is present in the catalysts.

FESEM analysis (Fig.3a-d) was carried out to obtain information about the grain size, the shape and the degree of particle agglomeration of the catalysts. The FESEM image of the BTOsg reveals that the particles of this material are in the micrometer size range and that they are formed by highly agglomerated irregular grains. This fact suggests that a sintering process of the mixed oxide occurred during the synthesis due to the high temperature used for the calcination step (850ºC for 6h), which is in agreement with the low surface area of the catalysts (Table 2). After the incoporation of copper into the perovskite (Cu-BTOsg), the morphology of the powder changes from agglomerated grains into needle-shape grains, although the grain size does not appreciably change (Fig.3b). For the BBOH and Cu-BBOH catalysts, a very different shape is observed by FESEM (Fig.3c-d) as well as a decrease of the grains size to the nanometer range. Both hydrothermal synthesized solids show grains with hollow cube morphology, but the shape of the Cu-BBOH catalyst is more irregular than that of the BBOH catalyst due to the understoichiometric amount of titanium used during the synthesis. Note that for Cu-BBOH particles different to the hollow cube are not distinguished, confirming that copper is highly dispersed on the surface of the BBOH perovskite.

III.3 Surface composition characterization by XPS

XPS was used to determine the near-surface composition and near-surface ion electronic states of Cu and O and the results are shown in Fig.4-5 and in Table 2. Fig.4 shows the XPS spectra obtained for the Cu $2p_{3/2}$ transition of Cu-BTOsg and Cu-BBOH catalysts. The deconvolution of the normalized spectra of Cu-BTOsg reveals two bands with binding energy (BE) maxima at 933.2 eV and 935.2 eV, corresponding to Cu (II) species, which is confirmed by the appearing of a satellite peak (not shown) at 941-944 eV, due to the presence of a free 3d level [53,54]. For the Cu-BBOH catalyst, the bands BE maxima appear at 932.2 eV and 934.1 eV, being the satellite

peak (not shown) at 941-944 eV and, consequently, also corresponding to Cu (II) species [43,55].

The position of the XPS bands corresponding to Cu (II) species reveals a stronger interaction between copper and the perovskite surface for the Cu-BTOsg catalyst than for the Cu-BBOH catalyst, since the maximum of the bands appears at higher BE for the former catalyst. Thus, the two contributions of the Cu-BTOsg catalyst can be ascribed to: i) copper with stronger interaction with support or incorporated into the structure (Cu_L at high eV) and ii) copper with weaker interaction with the support or supported copper (Cu_S at low eV) [37]. The Cu XPS spectra of the Cu-BBOH catalyst is the expected for supported copper oxide [30]. Additionally, by comparing the Cu/Ba+Ti+Cu ratio calculated from XPS data (shown in Table 2) with the corresponding nominal ratio for both catalysts, it can be deduced that: i) copper is incorporated into the catalyst structure of the Cu-BTOsg since the XPS ratio is lower than the nominal ratio and ii) copper is located on the catalyst surface of the Cu-BBOH because the Cu/Ba+Ti+Cu XPS ratio is higher than the nominal one. On the other hand, considering that the Ti/Ba ratio must be 1 for a $BaTiO_3$ perovskite and 0.5 for a Ba_2TiO_4 mixed oxide, the data of Table 2 reveal that for the BTOsg and Cu-BTOsg catalysts, the Ti/Ba and Ti+Cu/Ba ratios are close to 0.5 suggesting that the Ba_2TiO_4 phase is present at the surface of this catalyst due to the incorporation of copper into the perovskite structure [26]. On the contrary, for the BBOH and Cu-BBOH catalysts, the Ti/Ba and Ti+Cu/Ba ratios are closer to 1, indicating that $BaTiO_3$ is the main phase. Thus, in agreement with the XRD and Raman results, the XPS characterization also indicates that the incorporation of copper into the perosvkite structure only takes place when the sol-gel method is used.

13

Fig.5 shows the XPS spectra of the O1s transition for the BTOsg, BBOH, Cu-BTOsg and Cu-BBOH catalysts, where three contributions, at approximately 529 eV, 531 eV and 533 eV binding energies, are identified. According to literature [56,57], they can be ascribed to: i) lattice oxygen of metal oxides at ca. 529 eV (denoted as O_L), ii) surface oxygen species such as oxygen peroxides (O_2^{2-}), surface carbonates (CO_3^{2-}), and/or hydroxyl groups (OH^-), at ca. 531 eV (denoted as O*) and, iii) adsorbed water at ca. 533 eV (denoted as H_2O). For the bare perovskites (BTOsg and BBOH) the band corresponding to lattice oxygen (O_L) shows the highest intensity. This highlights the high crystallinity degree of both samples, although the BTOsg perovskite shows a higher concentration of surface oxygen species than the BBOH perovskite. These surface oxygen species of the BTOsg perovskite mostly correspond to carbonate species (also identified by XRD) formed by the carbonation of the segregated barium oxide, present at the end of the synthesis due to an incomplete reaction as previously mentioned [46]. After the copper addition (Cu-BTOsg and Cu-BBOH catalysts), the intensity of the band ascribed to surface oxygen species (O*) notably increases. Based on XRD and Raman results, it has been concluded that for the Cu-BTOsg a high segregation of phases, such as $BaCO_3$, Ba_2TiO_4, TiO_2 and CuO, occurs for the Cu-BTOsg perovskite due to the incorporation of copper into the perovskite structure. Thus, the band observed around 531 eV in the O1s XPS spectra of the Cu-BTOsg catalyst can be mostly ascribed to the presence of carbonate species on the catalyst surface. For the Cu-BBOH catalyst, the high intensity of the band at 531 eV seems to mainly correspond to the presence of a high amount of surface hydroxyl species, formed on the surface defects present in the perovskite structure due to the under stoichiometric amount of titanium used in the synthesis. This also explain the highest concentration of adsorbed water (band at 533 eV).

III.4 Temperature programmed reduction (H$_2$-TPR)

The reducibility of copper in the BaTi$_{0.8}$Cu$_{0.2}$O$_3$ catalysts prepared using both sinthesys methods has been analized by temperature programmed reduction with hydrogen (H$_2$-TPR) and the H$_2$ consumption profiles between 100 and 800ºC are shown in Fig.6. The Cu-BTOsg and Cu-BBOH catalysts show a well-defined H$_2$ consumption peak between 250 and 350ºC which corresponds to the reduction of almost all copper species as the percentage of reduced copper (included in Table 2) indicates [37]. The high H$_2$ consumption for the Cu-BBOH catalyst corresponds to the reduction of highly dispersed copper oxide on the BaTiO$_3$ surface which takes place at lower temperature than for the copper oxide used as reference (profile also included in Fig.6) [58,59]. For the Cu-BTOsg the high H$_2$ consumption peak at low temperature is ascribed to the reduction of copper incorporated into the lattice because this situation implies an increase in the copper coordination respect to the CuO used as reference, which increases copper reducibility. Moreover, the strong electronic interaction of copper with the other perovskite atoms also contributes to decrease the reduction temperature [37]. On the contrary, the H$_2$ consumption profiles of the Cu-BTOsg and Cu-BBOH between 350 and 800ºC are different. For the Cu-BTOsg, an increase of the TCD signal below 450ºC and two peaks at 380 and 800ºC are detected. The peak at ca. 380ºC corresponds to the reduction of an agglomerated copper oxide phase, also identified by XRD, as this reduction occurs at the same temperature than the copper oxide used as reference. The increase of the TCD signal at temperature higher than 450ºC corresponds to the desorption of surface oxygen species, such as hydroxyl at 450ºC, and to the decomposition of carbonate groups below 750ºC [37]. The profile of the Cu-BBOH catalyst shows a low H$_2$ consumption between 350 and 800ºC due to the desorption of surface oxygen (hydroxyl) species identified by XPS.

III.5. Catalytic activity: NOₓ storage and soot oxidation experiments under temperature programmed reaction (TPR) conditions.

The challenge for NOx and soot removal is to design a suitable low temperature catalyst with high stability, sulphur poisoning resistance and low cost. Fig.7 shows the NOx TPR conversion profiles for the BTOsg, Cu-BTOsg, BBOH, Cu-BBOH catalysts, which provide information about the NOx adsorption and desorption process. In these profiles a positive value of NOx conversion reveals that NOx adsorption occurs, whilst a negative percentage of NOx conversion indicates that NOx desorption is taking place. Thus, as it was expected, the BTOsg and BBOH catalysts show flat NOx conversion profiles, suggesting that NOx adsorption and desorption processes do not take place in an appreciably extent. As it has been previously reported [37,38], the amount of surface oxygen species plays an important role in the NOx storage capacity and the characterization results reveal that BTOsg and BBOH catalysts present a high crystalline structure with a small amount of defects and, for hence, a low amount of surface oxygen species, which explains their poor NOx adsorption/desorption capacity. After the addition of copper into the perovskite, a different performance for NOx adsorption and desorption has been observed. The Cu-BTOsg NOx conversion profile shows two adsorption maxima at around 300ºC and 450ºC -corresponding to two different adsorption processes- and one desorption minimum at around 560ºC [37]. For the Cu-BBOH catalyst, only a low NOx conversion minimum can be identified. The XPS and XRD results indicate that the Cu-BTOsg catalyst presents both a high amount of segregated phases ($BaCO_3$ and Ba_2TiO_4) and a high amount of surface oxygen species (mainly carbonate), due to the partial substitution of titanium by copper into the perovskite structure, which explains the high NOx adsorption capacity [37,38]. However, for the Cu-BBOH catalyst, copper was not incorporated into the perovskite structure remaining supported on the

catalyst surface as copper oxide and, for hence, a low NOx adsorption capacity is shown. However, the desorption observed in Fig.7 for Cu-BBOH reveals that some NOx must be adsorbed on the surface oxygen groups (hydroxyl) generated due to the under-stoichiometric amount of titanium used during synthesis. However, as the amount of surface oxygen species is much lower for Cu-BBOH than for Cu-BTOsg, a lower NOx adsorption/desorption is observed.

The TPR NO_2 profiles corresponding to the NOx adsorption-desorption experiments shown in Fig.8 provide information about the catalysts activity for the NO oxidation to NO_2. At low temperature all the catalysts seem to accelerate the NO oxidation to NO_2, but beyond 550ºC the NO_2 percentage decreases due to thermodynamic limitations. The NO_2 production is notably higher for both catalysts in the presence of copper due to its ability for the catalysis of this oxidation reaction [43]. However, again, the location of copper in the perovskite structure determines the catalytic performance, showing the Cu-BBOH catalyst the highest activity for the NO oxidation to NO_2 (around 30% of NO_2 production between 400 and 450ºC), due to the presence of highly dispersed copper oxide on the catalyst surface. When copper is introduced into the perovskite structure (Cu-BTOsg), the NO_2 production is also improved respect to BTOsg due to the presence of a small amount of surface CuO, but the increase is apparently lower than for the Cu-BBOH catalyst. In the NO_2 profile of the Cu-BTOsg catalyst, it is also observed a minimum at the temperature at which the NOx adsorption profile (Fig.7) achieves the maximum because a fraction of the NO_2 generated is being adsorbed on the active sites created due to the incorporation of copper into the perovskite structure. Consequently, the high NOx adsorption capacity of the Cu-BTOsg catalyst decreases the observed NO to NO_2 oxidation activity

According to the NO to NO_2 oxidation activity shown by the copper perovskite catalysts, the soot oxidation activity in NO/O_2 atmosphere of these catalysts has been also tested. Fig.9

features the soot oxidation TPR profiles obtained, including the corresponding to BTOsg and BBOH perovskites and a model platinum catalyst for comparative purposes, whilst Table 3 presents the related data (T50% -which is the temperature required to convert 50% of the soot used in each experiment- and the percentage of selectivity to CO_2). The data indicate that only in the presence of copper the temperature for soot oxidation (T 50%) decreases and the CO_2 selectivity of the catalyst increases. As it was expected considering the NO_2 profiles (Fig.8), Cu-BBOH -with copper highly dispersed on the surface- is the most active catalyst for soot oxidation in NO/O_2 atmosphere since it shows the lowest soot combustion temperature and also the highest selectivity to CO_2 (93% CO_2 selectivity) which is close to that shown by the model platinum catalyst.

Thus, it can be concluded that the location of copper in the catalyst determines the catalytic activity and, hence, its application. When copper is incorporated into the perovskite structure, a catalyst with a high NOx storage capacity is obtained, but if copper remains as highly dispersed copper oxide on the surface of $BaTiO_3$, the catalyst shows a high activity for the NO to NO_2 oxidation and, therefore, can be used as an oxidation catalyst for soot removal.

IV. Conclusions

From the results presented in this paper, the following conclusions can be extracted:

- $BaTiO_3$ and $BaTi_{0.8}Cu_{0.2}O_3$ perovskites with tetragonal structure have been synthesized using both sol-gel and the hydrothermal method. For the hydrothermal method, barium hydroxide is the most convenient barium precursor because it avoids the use of an additional alkaline mineralizer.

18

- The position of copper on the catalyst is highly dependent of the synthesis method: i) for sol-gel method, the copper is partially introduced into the perovskite structure, promoting the segregation of phases, distorting the perovskite structure and creating oxygen vacancies which allows the formation of a high amount of oxygen surface groups and ii) for hydrothermal method, the copper remains highly dispersed on the surface of the perovskite which, in turn, shows a higher degree of crystallinity and a lower amount of oxygen surface groups than the former method.

- The location of copper in the catalyst determines its catalytic applications: the sol-gel catalyst (Cu-BTOsg), with copper incorporated into the perovskite structure, presents a high NOx storage capacity whilst the hydrothermal catalyst (Cu-BBOH), with copper highly dispersed on the surface, shows a high activity for the NO oxidation to NO_2 and, hence, can be used as catalyst for soot removal.

V. Acknowledgements.

VI. References

[1]   R. Kavian, A. Saidi, J. Alloys Compd. 468 (2009) 528–532.

[2]   A S. Bhalla, R. Guo, R. Roy, Mater. Res. Innov. 4 (2000) 3–26.

[3]   H. Kaddoussi, Y.G.A. Lahmar, B.A.J.L. Dellis, J. Mater. Sci. 51 (2016) 3454–3462.

[4]   H. Nagamoto, K. Amanuma, H. Nobutomo, H. Inoue, Chem. Lett. 17 (1988) 237–240.

[5]   X. Li, Q. Hu, Y. Yang, Y. Wang, F. He, Appl. Catal. A Gen. 413-414 (2012) 163–169.

[6]   R. Shiozaki, A.G. Andersen, T. Hayakawa, S. Hamakawa, K. Suzuki, M. Shimizu, K. Takehira, J. Chem. Soc. Trans. 93 (1997) 3235–3242.

[7]   D. Duprez, F. Can, X. Courtois, C. Batiot-dupeyrat, S. Laassiri, H. Alamdari, Chem. Rev. 114 (2014) 10292-10368.

[8]   J.P. Zou, L.Z. Zhang, S.L. Luo, L.H. Leng, X.B. Luo, M.J. Zhang, Y. Luo, G.C. Guo, Int. J. Hydrogen Energy 37 (2012) 17068–17077.

[9]   W.J. Liang, L. Ma, H. Liu, J. Li, Chemosphere 92 (2013) 1390–1395.

[10]   G. Ciofani, S. Danti, S. Moscato, L. Albertazzi, D. D'Alessandro, D. Dinucci, F. Chiellini, M. Petrini, A Menciassi, Colloids Surf. B. Biointerfaces 76 (2010) 535–43.

[11]   D. Kim, Microw. Opt. Technol. Lett. 54 (2012) 2781–2784.

[12]   M. A. Peña, J.L.G. Fierro, Chem. Rev. 101 (2001) 1981–2017.

[13]   V. Rives, in:, Wiley-VCH Verlag GmbH & Co. KGaA, Perovskites Relat. Mix. Oxides, Weinheim 2016, pp. 1–24.

[14] M. Boulos, S. Guillemet-Fritsch, F. Mathieu, B. Durand, T. Lebey, V. Bley, Solid State Ionics 176 (2005) 1301–1309.

[15] A. Testino, M.T. Buscaglia, V. Buscaglia, M. Viviani, C. Bottino, P. Nanni, Chem. Mater. 16 (2004) 1536–1543.

[16] J. Wang, J. Fang, S. Ng, L. Gan, C. Chew, X. Wang, Z. Shen, J. Am. Ceram. Soc. 81 (1999) 873–881.

[17] Z. Deng, Y. Dai, H. Xiao, M.J. Zhou, Adv. Mater. Res. 1004-1005 (2014) 63–68.

[18] J. Chen, S.Q. Li, M.C. Che, W.D. Yi, Adv. Appl. Ceram. 114 (2015) 150–155.

[19] S. Lee, T. Son, J. Yun, H. Kwon, G.. Messing, B. Jun, Mater. Lett. 58 (2004) 2932–2936.

[20] L. Simon-Seveyrat, A. Hajjaji, Y. Emziane, B. Guiffard, D. Guyomar, Ceram. Int. 33 (2007) 35–40.

[21] S.K. Tripathy, T. Sahoo, M. Mohapatra, S. Anand, R.P. Das, Mater. Lett. 59 (2005) 3543–3549.

[22] N. Sasirekha, B. Rajesh, Ind. Eng. Chem. Res. 47 (2008) 1868–1875.

[23] H. Xu, L. Gao, J. Guo, J. Eur. Ceram. Soc. 22 (2002) 1163–1170.

[24] L. Qi, B.I. Lee, P. Badheka, L.Q. Wang, P. Gilmour, W.D. Samuels, G.J. Exarhos, Mater. Lett. 59 (2005) 2794–2798.

[25] R.E. Riman, Chem. Mater. 5 (1993) 61–70.

[26] D.R. Modeshia, R.I. Walton, Chem. Soc. Rev. 39 (2010) 4303-4325.

[27] B. Newalkar, Mater. Res. Bull. 36 (2001) 2347–2355.

[28] L. Guo, H. Luo, J. Gao, L. Guo, J. Yang, Mater. Lett. 60 (2006) 3011–3014.

[29] Y. Kobayashi, A. Nishikata, T. Tanase, M. Konno, J. Sol-Gel Sci. Technol. 29 (2004) 49–55.

[30] H. Shimooka, K. Yamada, S. Takahashi, Ratio 876 (1998) 873–876.

[31] A. Kareiva, S. Tautkus, R. Rapalaviciute, J. Mater. 34 (1999) 4853 – 4857.

[32] J.B. Liu, W.-C. Li, Z.M. Wang, C.P. Zheng, Mater. Sci. Technol. 17 (2001) 606–608.

[33] T. Sahoo, S.K. Tripathy, M. Mohapatra, S. Anand, R.P. Das, Mater. Lett. 61 (2007) 1323–1327.

[34] N. Bao, L. Shen, G. Srinivasan, K. Yanagisawa, A. Gupta, J. Phys. Chem. C 112 (2008) 8634–8642.

[35] P. Ciambelli, S. Cimino, L. Lisi, M. Faticanti, G. Minelli, I. Pettiti, P. Porta, Appl. Catal. B Environ. 33 (2001) 193–203.

[36] F.N. Agüero, M.R. Morales, S. Larrégola, E.M. Izurieta, E. Lopez, L.E. Cadús, Int. J. Hydrogen Energy 40 (2015) 15510–15520.

[37] V. Albaladejo-Fuentes, F.E. López-Suárez, M.S. Sánchez-Adsuar, M.J. Illán-Gómez, Appl. Catal. A Gen. 488 (2014) 189–199.

[38] F.E. López-Suárez, S. Parres-Esclapez, A. Bueno-López, M.J. Illán-Gómez, B. Ura, J. Trawczynski, Appl. Catal. B Environ. 93 (2009) 82–89.

[39] F.E. López-Suárez, M.J. Illán-Gómez, A. Bueno-López, J.A. Anderson, Appl. Catal. B-Environ. 104 (2011) 261–267.

[40] M. V. Twigg, Appl. Catal. B Environ. 70 (2007) 2–15.

[41] W.S. Epling, L.E. Campbell, A. Yezerets, N.W. Currier, J.E. Parks, Catal. Rev. 46 (2004) 163–245.

[42] Z. Liu, S. Ihl Woo, Catal. Rev. 48 (2006) 43–89.

[43] F.E. López-Suárez, A. Bueno-López, M.J. Illán-Gómez., Appl. Catal. B Environ. 84 (2008) 651–658.

[44] G. Fan, L. Zhao, C. Gong, J. Ma, G. Xue, Nano 11 (2016) 1650010-1-1650010-7.

[45] F. Xia, J. Liu, D. Gu, P. Zhao, J. Zhang, R. Che, Nanoscale 3 (2011) 3860–3867.

[46] C. Blanco, G. Fourlaris, B. Rand, F.L. Riley, J. Am. Ceram. Soc. 86 (1999) 1777–1786.

[47] J.I. Langford, A.J.C. Wilson, J. Appl. Crystallogr. 11 (1978) 102–113.

[48] S.G. Kwon, B.H. Park, K. Choi, E.S. Choi, S. Nam, J.W. Kim, J.H. Kim, J. Eur. Ceram. Soc. 26 (2006) 1401–1404.

[49] H. Hayashi, T. Nakamura, T. Ebina, J. Phys. Chem. Solids 74 (2013) 957–962.

[50] R. Asiaie, W.D. Zhu, S.A. Akbar, P.K. Dutta, Chem. Mater. 8 (1996) 226–234.

[51] M. Rössel, H.-R. Höche, H.S. Leipner, D. Völtzke, H.-P. Abicht, O. Hollricher, J. Müller, S. Gablenz, Anal. Bioanal. Chem. 380 (2004) 157–162.

[52] G. Guo, K. Lian, F. Gu, D. Han, Z. Wang, Chem. Commun. 50 (2014) 13575–13577.

[53] J. Ghijsen, L. Tjeng, J. van Elp, H. Eskes, J. Westerink, G. Sawatzky, M. Czyzyk, Phys. Rev. B 38 (1988) 11322–11330.

[54] F.E. López-Suárez, A. Bueno-López, M.J. Illán-Gómez, J. Trawczynski, Appl. Catal. A Gen. 485 (2014) 214–221.

[55] A. Arango-Díaz, E. Moretti, A. Talon, L. Storaro, M. Lenarda, P. Núñez, J. Marrero-Jerez, J. Jiménez-Jiménez, A. Jiménez-López, E. Rodríguez-Castellón, Appl. Catal. A Gen. 477 (2014) 54–63.

[56] D.Y. Yoon, E. Lim, Y.J. Kim, J.H. Kim, T. Ryu, S. Lee, B.K. Cho, I.-S. Nam, J.W. Choung, S. Yoo, J. Catal. 319 (2014) 182–193.

[57] S. Ponce, M.. Peña, J.L. Fierro, Appl. Catal. B Environ. 24 (2000) 193–205.

[58] L. Dong, Y. Hu, M. Shen, T. Jin, J. Wang, W. Ding, Y. Chen, Chem. Mater. 13 (2001) 4227–4232.

[59] G. Avgouropoulos, T. Ioannides, H. Matralis, Appl. Catal. B Environ. 56 (2005) 87–93.

Table 1. Nomenclature, molecular composition and synthesis details of the catalysts.

Catalyst	Synthesis method	Molecular composition	Barium precursor	Mineralizer
BTOsg	Sol-gel	$BaTiO_3$	Barium acetate	Not needed
BAKOH	Hydrothermal	$BaTiO_3$	Barium acetate	KOH
BASOH	Hydrothermal	$BaTiO_3$	Barium acetate	NaOH
BNKOH	Hydrothermal	$BaTiO_3$	Barium nitrate	KOH
BNSOH	Hydrothermal	$BaTiO_3$	Barium nitrate	NaOH
BBOH	Hydrothermal	$BaTiO_3$	Barium hydroxide	Not added
Cu-BTOsg	Sol-gel	$BaTi_{0.8}Cu_{0.2}O_3$	Barium acetate	Not needed
Cu-BAKOH	Hydrothermal	$BaTi_{0.8}Cu_{0.2}O_3$	Barium acetate	KOH
Cu-BASOH	Hydrothermal	$BaTi_{0.8}Cu_{0.2}O_3$	Barium acetate	NaOH
Cu-BNKOH	Hydrothermal	$BaTi_{0.8}Cu_{0.2}O_3$	Barium nitrate	KOH
Cu-BNSOH	Hydrothermal	$BaTi_{0.8}Cu_{0.2}O_3$	Barium nitrate	NaOH
Cu-BBOH	Hydrothermal	$BaTi_{0.8}Cu_{0.2}O_3$	Barium hydroxide	Not added

Table 2. Characterization data for BTOsg, Cu-BTOsg, BBOH and Cu-BBOH catalysts.

Catalyst	S_{BET} (m^2/g)	Nominal Cu (wt%)	ICP-AES Cu (wt%)	Average crystal size (nm)	a (Å)	c (Å)	FWHM (2 0 0)/ (1 1 1)	Cu reduced during H$_2$-TPR (molar %)*	Cu/ Cu+Ba+Ti (nominal)	Cu/ Cu+Ba+Ti (XPS)	Ti/ Ba (XPS)	Ti+Cu /Ba (XPS)
BTOsg	9	-	-	29	4.011	4.005	1.48	-	-	-	0.55	-
Cu-BTOsg	11	5.4	5.4	38	4.008	4.008	1.44	-	-	-	0.92	-
BBOH	11	-	-	37	4.007	4.007	1.70	93	0.1	0.08	-	0.49
Cu-BBOH	15	5.4	5.5	34	4.001	4.004	1.52	98	0.1	0.12	-	0.98

Experiment carried out under a 5% H$_2$/Ar flow (40 ml/min, Ptotal = 1 atm) in temperature programmed conditions from 25ºC to 900ºC at 10ºC/min

Table 3. T50% (Temperature for the 50% soot conversion) and CO_2 selectivity obtained for the BTOsg, Cu-BTOsg, BBOH, Cu-BBOH catalysts and for Pt/Al_2O_3 as reference.

Catalyst	T50% (ºC)	CO_2 selectivity (%)
No catalyst	591	38
BTOsg	594	46
BBOH	585	38
Cu-BTOsg	565	70
Cu-BBOH	545	93
Pt/Al_2O_3	492	99

Experiments carried out under a gas flow containing 500 ppm NOx and 5% O_2 in N_2 balance (500 ml/min, Ptotal = 1 atm) in temperature programmed conditions from 25ºC to 800ºC at 10ºC/min.

Fig. 1 XRD diffractograms for the sol-gel and hydrothermal: a) $BaTiO_3$ catalysts and b) $BaTi_{0.8}Cu_{0.2}O_3$ catalysts. ▼ $BaTiO_3$, ◊$Ba_2SiTi_2O_8$, □ Ba_2TiO_4, ♦ $BaCO_3$, ■ TiO_2, ● CuO.
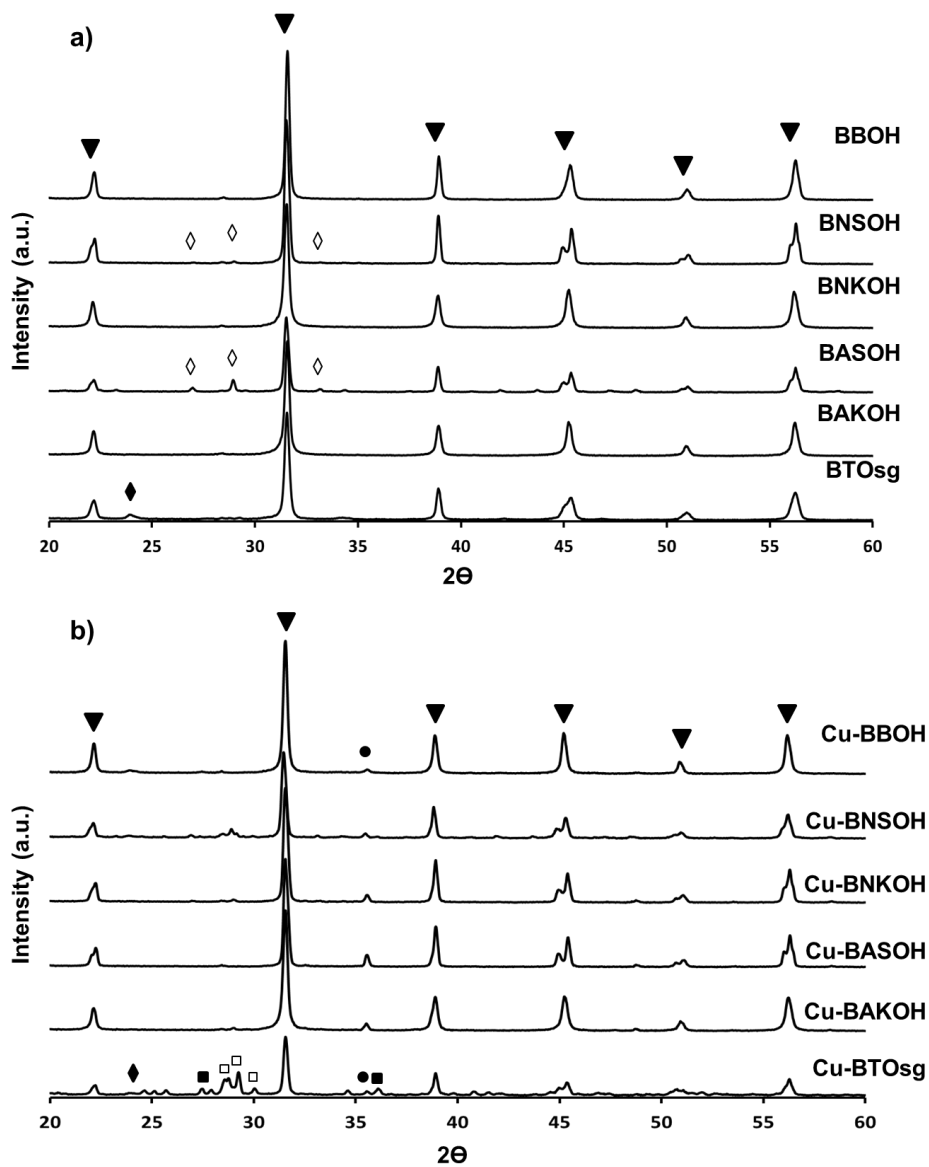
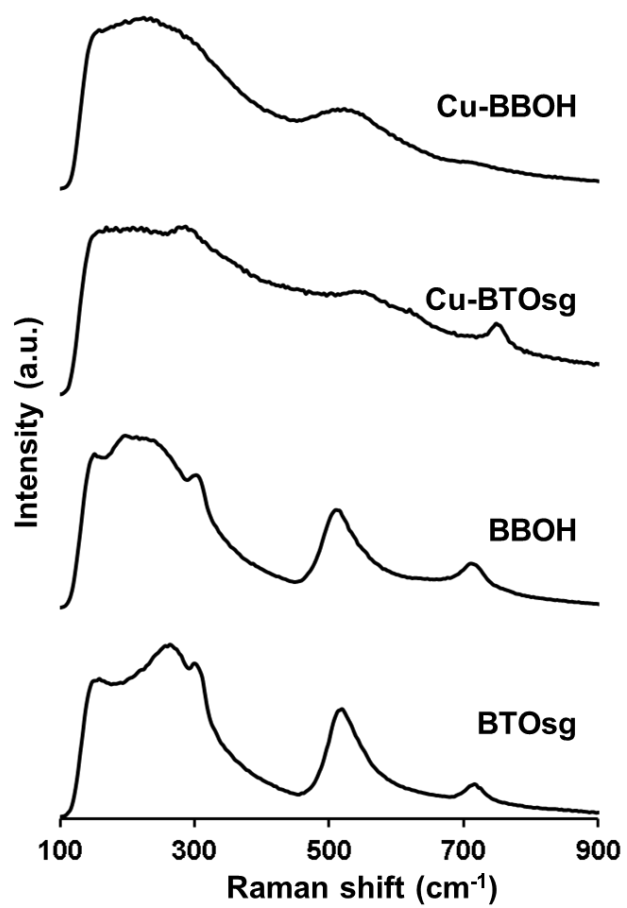**Fig. 2.** Raman spectra for BTOsg, Cu-BTOsg, BBOH and Cu-BBOH catalysts.

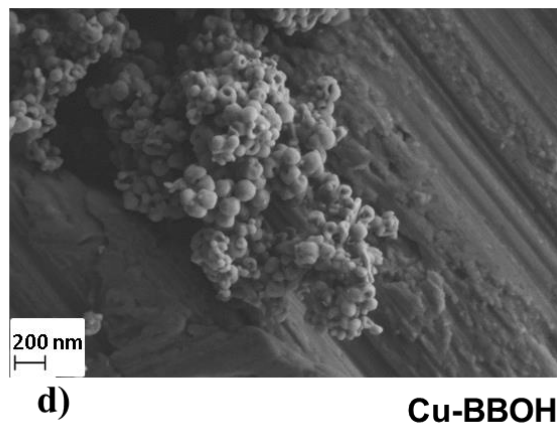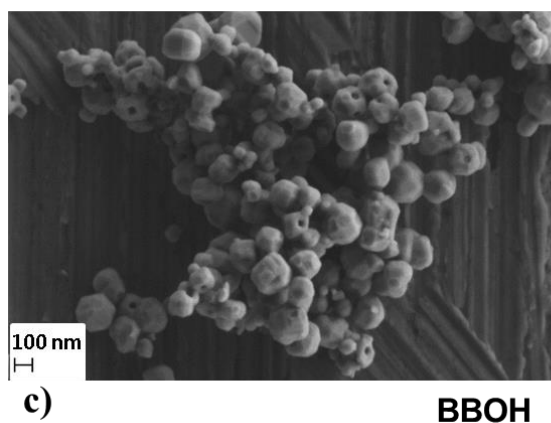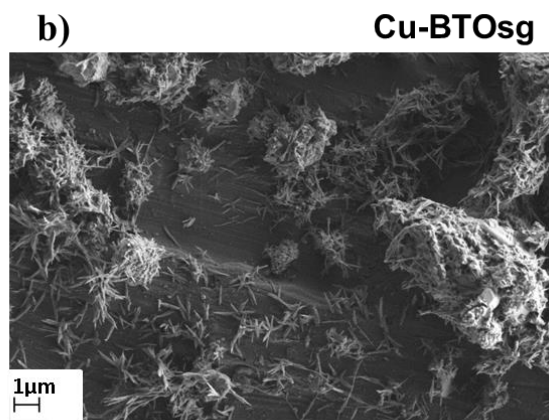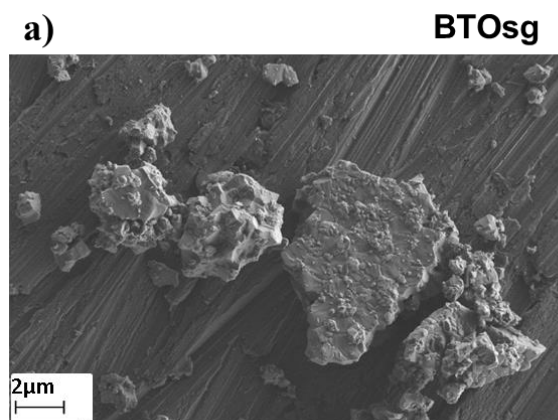**Fig. 3** a-d FESEM images for BTOsg, Cu-BTOsg, BBOH and Cu-BBOH catalysts.

Fig. 4. Cu $2p_{3/2}$ XPS spectra for Cu-BTOsg and Cu-BBOH catalysts.
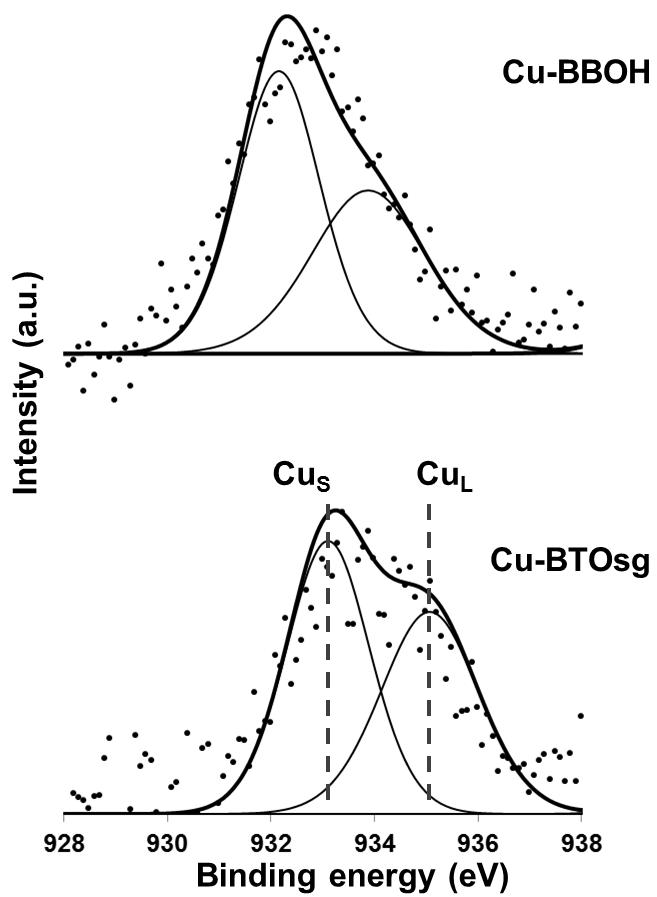
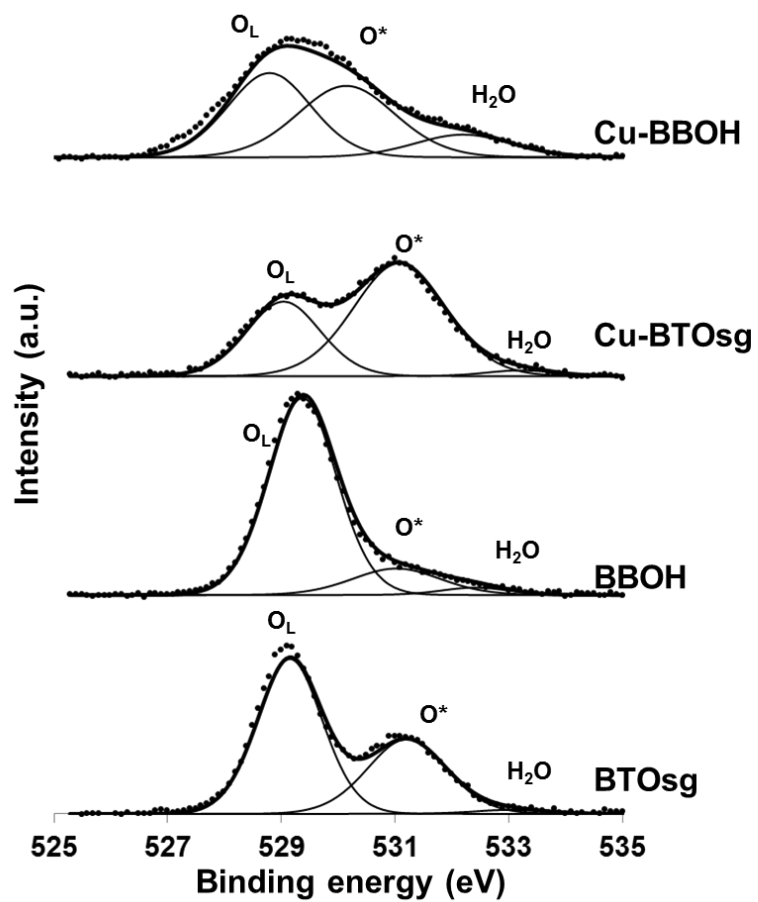**Fig. 5.** O1s XPS transition for BTOsg, Cu-BTOsg, BBOH and Cu-BBOH catalysts.

Fig. 6. TPR-H_2 profiles for CuO ref, Cu-BTOsg and Cu-BBOH catalysts. (Experiments carried out under a gas flow (40 ml/min, Ptotal = 1 atm) containing 5% H_2 in Ar balance).

Fig. 7. TPR NOx conversion profiles (%) for BTOsg, Cu-BTOsg, BBOH and Cu-BBOH catalysts (Experiments carried out under a gas flow (500 ml/min, Ptotal = 1 atm) containing 500 ppm NOx and 5% O_2 in N_2 balance).

Fig. 8. TPR NO_2 generation profiles for BTOsg, Cu-BTOsg, BBOH and Cu-BBOH catalysts (Experiments carried out under a gas flow (500 ml/min, Ptotal = 1 atm) containing 500 ppm NOx and 5% O_2 in N_2 balance).

Fig. 9. TPR soot conversion profiles (%) for BTOsg, Cu-BTOsg, BBOH, Cu-BBOH catalysts and Pt/Al_2O_3 as reference (Experiments carried out under a gas flow (500 ml/min, Ptotal = 1 atm) containing 500 ppm NOx and 5% O_2 in N_2 balance).

Fig. 1 XRD diffractograms for the sol-gel and hydrothermal: a) BaTiO$_3$ catalysts and b) BaTi$_{0.8}$Cu$_{0.2}$O$_3$ catalysts.

▼ **BaTiO$_3$,** ◇**Ba$_2$SiTi$_2$O$_8$,** □ **Ba$_2$TiO$_4$,** ◆ **BaCO$_3$,** ■ **TiO$_2$,** ● **CuO.**

Fig. 2. Raman spectra for BTOsg, Cu-BTOsg, BBOH and Cu-BBOH catalysts.

Fig. 3 a-d FESEM images for BTOsg, Cu-BTOsg, BBOH and Cu-BBOH catalysts.

Fig. 4. Cu $2p_{3/2}$ XPS spectra for Cu-BTOsg and Cu-BBOH catalysts.

Fig. 5. O1s XPS transition for BTOsg, Cu-BTOsg, BBOH and Cu-BBOH catalysts.

Fig. 6. TPR-H$_2$ profiles for CuO ref, Cu-BTOsg and Cu-BBOH catalysts. (Experiments carried out under a gas flow (40 ml/min, Ptotal = 1 atm) containing 5% H$_2$ in Ar balance).
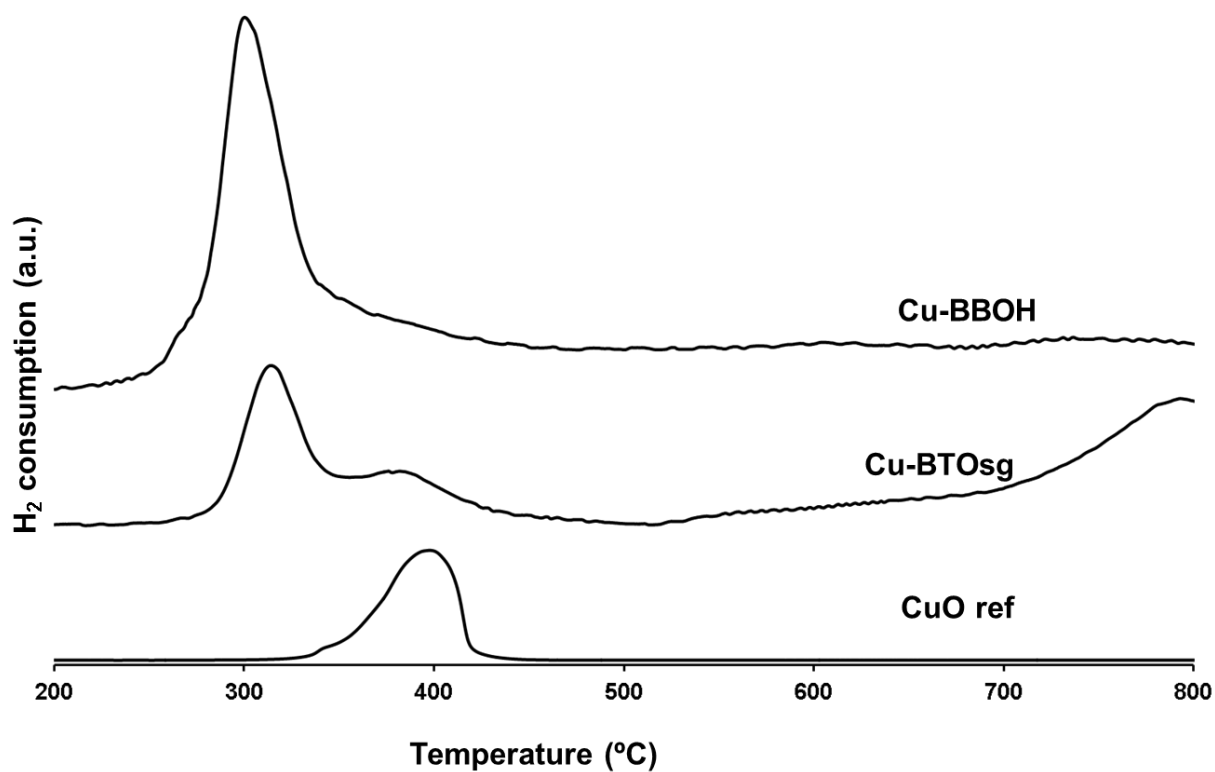
Fig. 7. TPR NOx conversion profiles (%) for BTOsg, Cu-BTOsg, BBOH and Cu-BBOH catalysts (Experiments carried out under a gas flow (500 ml/min, Ptotal = 1 atm) containing 500 ppm NOx and 5% O_2 in N_2 balance).
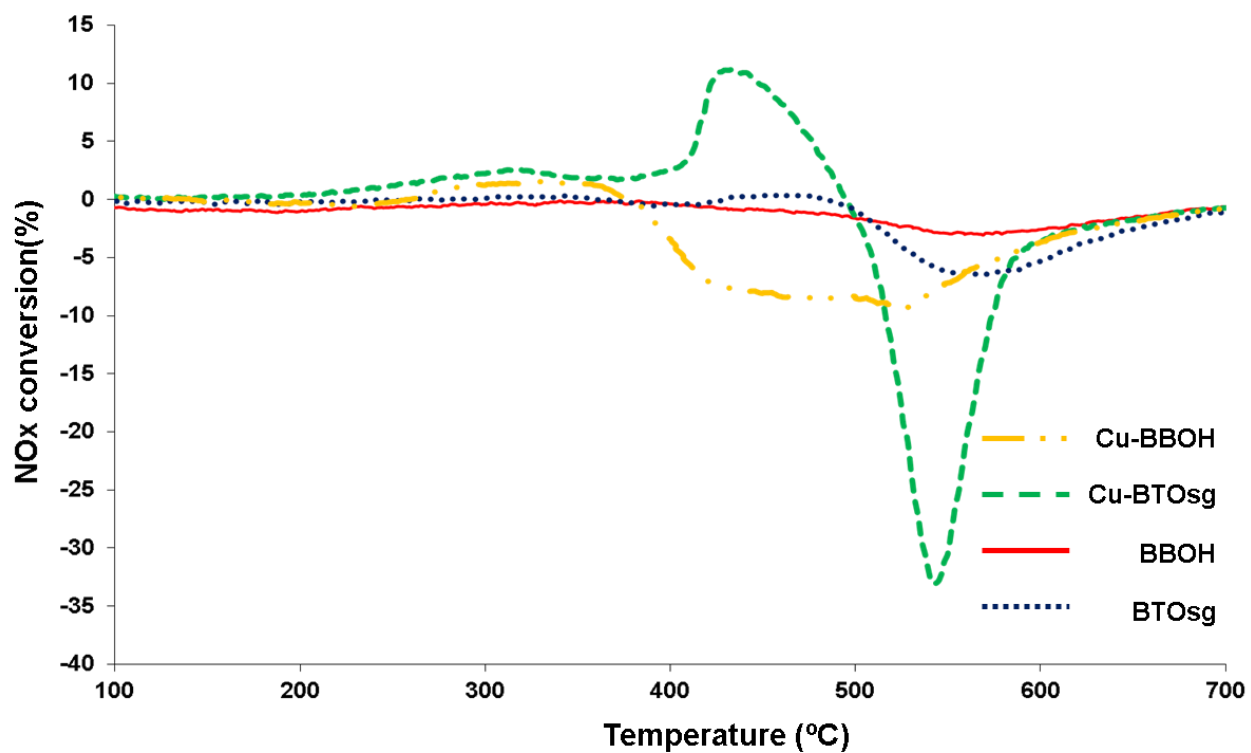
Fig. 8. TPR NO$_2$ generation profiles for BTOsg, Cu-BTOsg, BBOH and Cu-BBOH catalysts (Experiments carried out under a gas flow (500 ml/min, Ptotal = 1 atm) containing 500 ppm NOx and 5% O$_2$ in N$_2$ balance).
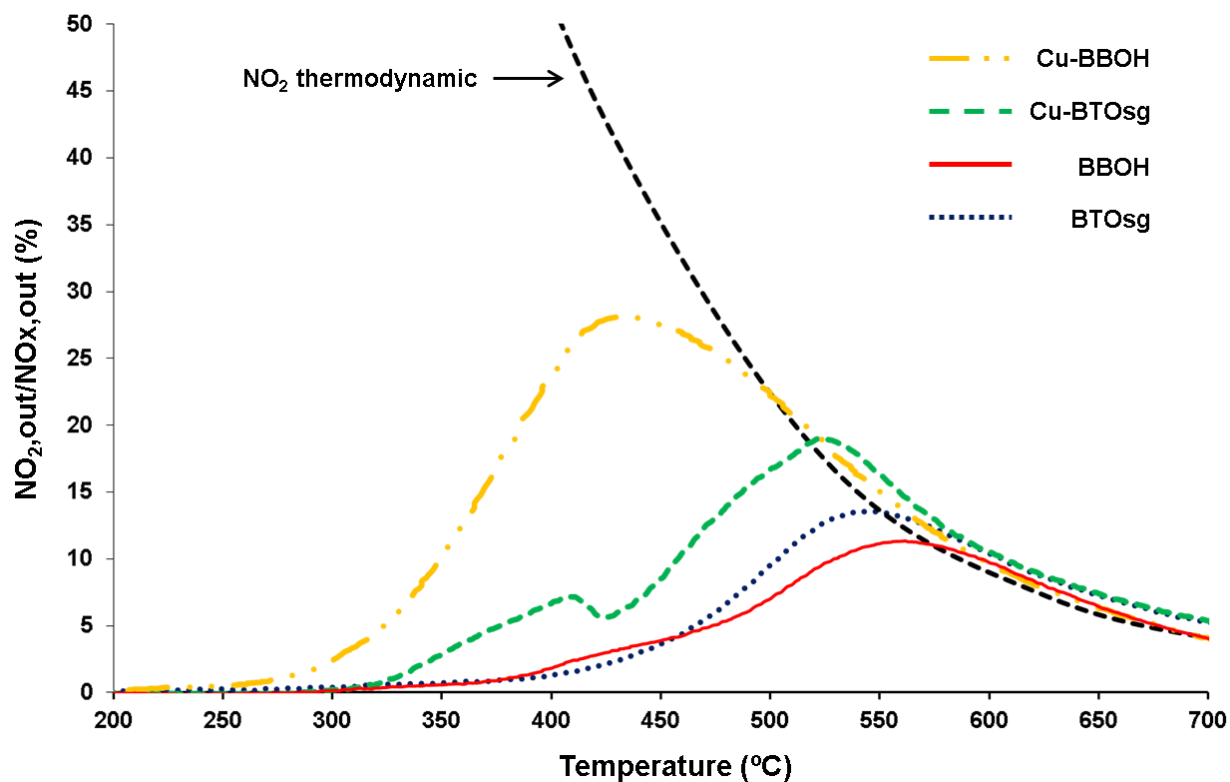
Fig. 9. TPR soot conversion profiles (%) for BTOsg, Cu-BTOsg, BBOH, Cu-BBOH catalysts and Pt/Al_2O_3 as reference (Experiments carried out under a gas flow (500 ml/min, Ptotal = 1 atm) containing 500 ppm NOx and 5% O_2 in N_2 balance).